Origin and fate of dissolved inorganic carbon in a karst groundwater fed peatland using δ13CDIC

Alexandre Lhosmot, Marc Steinmann, Philippe Binet, Laure Gandois, Jean-Sébastien Moquet, Vanessa Stefani, Marie-Laure Toussaint, Anne Boetsch, Christophe Loup, Valentin Essert, et al.

Chemical Geology xxx (xxxx) 121254

Contents lists available at ScienceDirect

Chemical Geology

journal homepage: www.elsevier.com/locate/chemgeo

Origin and fate of dissolved inorganic carbon in a karst groundwater fed peatland using $\delta^{13}C_{DIC}$

Alexandre Lhosmot [a,*], Marc Steinmann [a], Philippe Binet [a], Laure Gandois [b], Jean-Sébastien Moquet [c], Vanessa Stefani [a], Marie-Laure Toussaint [a], Anne Boetsch [a], Christophe Loup [a], Valentin Essert [a], Guillaume Bertrand [a]

[a] Chrono-Environnement, Université de Bourgogne Franche-Comté, UMR6249, CNRS, France
[b] EcoLab, Université de Toulouse, CNRS, France
[c] Institut des Sciences de la Terre d'Orléans (ISTO), Université d'Orléans, UMR7327, CNRS, France

ARTICLE INFO

Editor: Michael E. Boettcher

Keywords:
Peatland
Carbon-13
Jura Mountains
Karst
Methanogenesis
Groundwater dependent ecosystems

ABSTRACT

Continental hydrosystems and in particular peatlands play an important role in the carbon cycle of the Critical Zone (CZ). Peatlands are important sinks for organic carbon and have therefore been extensively studied. However, peatlands are not only important for the fate of organic carbon, but they also affect the cycle of Dissolved Inorganic Carbon (DIC) of the peatland and the surrounding watershed. The fate of DIC is particularly complex in peatlands in limestone-dominated regions, because bicarbonate concentrations in surface and groundwater are high and the interaction between peatlands and surrounding hydrosystems are facilitated by the presence of highly permeable karst aquifers. In the present paper we study the origin and the fractionation of DIC in a peatland located on top of a karst aquifer. The study is based on hydrochemical and isotopic ($\delta^{13}C_{DIC}$) data from samples recovered during 2 campaigns (low flow, high flow) at various depths within the Forbonnet peatland (Jura Mountains, eastern France), at the peatland outlet and at adjacent karst springs representing the underlying aquifer. In order to evaluate secondary fractionation processes, the measured $\delta^{13}C_{DIC}$ compositions were compared to modeled values considering the origin of DIC and potentially associated fractionation and speciation processes. The main results are: (1) DIC is lost at the bog surface by CO_2 outgassing. (2) The $\delta^{13}C_{DIC}$ compositions of deep catotelm pore waters from the bog were much heavier than the modeled values. We relate this discrepancy to methanogenesis and show that this process is favored by reduced conditions at pH ~ 6 and a HCO_3^- content of ~1 mmol/L, most probably due to punctual groundwater inflows at the base of the bog. Finally, contrasted $\delta^{13}C_{DIC}$ compositions between the bog and the fen of the peatland reveal an additional ecohydrological control on DIC speciation.

1. Introduction

The Critical Zone (CZ) is defined as the Earth's surface layer from the unweathered bedrock to the top of the canopy (Anderson et al., 2004). It hosts various biogeochemical cycles (Gaillardet et al., 2018; National Research Council, 2001) and among them the Earth's superficial cycle of carbon. Peatlands comprise 30% of the world's soils organic carbon stock (500 Gt; Gorham, 1991; Loisel et al., 2021) but represent only 3% of the global continental surface. Peatlands are thus hot spots of carbon cycling. At the watersheds scale they are the main contributors for organic carbon to surface water (Laudon et al., 2011; Rosset et al., 2019a, 2019b).

In contrast the importance of peatlands for fluxes of inorganic carbon and in particular of dissolved inorganic carbon (DIC) and related exchange mechanisms at the interface between lithosphere, hydrosphere and atmosphere remains poorly documented, although they could significantly contribute to the inorganic carbon balance at the watershed scale (Billett et al., 2014; Dinsmore et al., 2010). For instance, Wallin et al. (2010) showed in northern Sweden that the DIC concentration of stream water was positively correlated with the peatland coverage of their catchments, suggesting that water/rock interaction at catchment scale is related to the acidity produced in peatlands. This effect is even stronger in carbonate regions due to the high solubil-

* Corresponding author.
E-mail address: alexandre.lhosmot@univ-fcomte.fr (A. Lhosmot).

https://doi.org/10.1016/j.chemgeo.2022.121254
Received 3 March 2022; Received in revised form 3 May 2022; Accepted 30 November 2022
0009-2541/

ity of limestone compared to other rock types (Calmels et al., 2014; Fierz and Monbaron, 1999).

Nevertheless, peatlands are not only expected to contribute to the DIC cycle of the downstream areas, but they are also receptors of water and solutes, including DIC, from upstream (Bourbonniere, 2009; Chasar et al., 2000; Komor, 1994; Lamers et al., 1999). As they are mostly acid and reduced ecosystems, incoming DIC to peatlands will be subject to phase change and/or join the organic carbon cycle through CO_2 reduction associated to methane production (Alstad and Whiticar, 2011).

DIC content and isotopic signatures in natural water results from a varied panel of sources (carbonate, organic matter) and sinks (CO_2 outgassing, precipitation) of DIC and fractionation from chemical and biogeochemical reactions (Wigley et al., 1978). As a result, DIC in peatlands has multiple origins and is dependent on numerous processes (Campeau et al., 2017) summarized below:

(1) DIC is formed in peatlands by various processes, in particular as CO_2 produced by aerobic (surface) and anaerobic (deep) microbial degradation of organic matter (Limpens et al., 2008; Zhong et al., 2020; Corbett et al., 2013; Steinmann et al., 2008; Ye et al., 2012).
(2) In anaerobic peat layers, two main methanogenesis pathways affect the DIC dynamics: (1) the Acetoclastic Methanogenesis (AM) (Steinmann et al., 2008) and (2) the Hydrogenotrophic Methanogenesis (HM) that both produce CO_2 and CH_4 in equimolar proportion when considering all reactions (Corbett et al., 2013; Neumann et al., 2016). The relative contribution of these pathways is variable and controlled by diverse biotic and abiotic factors (Alstad and Whiticar, 2011; Conrad, 2020; Galand et al., 2005; Throckmorton et al., 2015).
(3) DIC, mainly in the form of bicarbonate (HCO_3^-), may be produced in situ by interaction of acidic peatland water with bedrock or may be imported by water inflows from upstream areas (Billett et al., 2014; Chasar et al., 2000). Both native and allochthonous DIC are particularly important in carbonate dominated regions due to the high solubility of limestone (Goldscheider et al., 2020; Sullivan et al., 2019).

Within this general scheme, peatland ecosystems can be conceptualized as biogeochemical reactors constrained by a wide range of hydrometeorological, geological and ecological parameters affecting the exchange of carbon between the ecosystem (living matter), the hydrosystem (DIC and dissolved/particulate organic carbon) and the atmosphere (gaseous exchanges) (Bernard-Jannin et al., 2018; D'Angelo et al., 2021; Rosset et al., 2019a, 2019b).

As mentioned before, DIC fluxes in peatlands are of particular importance in carbonate dominated regions. Although carbonate regions account for 15 to 20% of the ice-free continental surface (Goldscheider et al., 2020; Hartmann and Moosdorf, 2012), Martin et al. (2021) reported that CZ studies in carbonate regions are underrepresented. Moreover, limestone weathering is highly sensitive to climate change and anthropogenic disturbances (Sullivan et al., 2019). Consequently, by receiving DIC from upstream, recycling and producing DIC within peatlands, and by exporting acidity and DIC downstream, peatlands in carbonate regions could, in addition to their role as organic carbon sinks, also constitute key ecosystems for continental DIC cycles. Despite there is to our knowledge no quantitative surface estimation of peatlands under carbonate influence, these ecosystems are specific from an ecological perspective (e.g. "Calcareous fen"). In addition, overlaying the global peatland map (Xu et al., 2018) on the worldwide carbonate bedrock distribution map (Goldscheider et al., 2020) reveals that high peatland densities occur in carbonate areas, especially in the northern hemisphere such as UK, Siberia or western China.

In order to propose a typology of these possible interactions, we studied the water chemistry and the isotopic signature of DIC in a peatland in the French Jura Mountains by combining upstream-downstream gradients, vertical profiles and contrasting hydrological settings (low flow/high flow). More specifically, our objectives were (i) to assess DIC fluxes from the peatland to the atmosphere (vertical gradient); (ii) to evaluate the consequences of the carbonated groundwater inflows on DIC speciation mechanisms (hydrogeological gradient) within the peatland; and (iii) to document potential ecohydrological constraints (bog-fen gradients) for DIC speciation. From these evaluations, a conceptual typology of mechanisms affecting DIC patterns in peatlands in carbonate regions will be proposed followed by some perspectives for future research.

2. Context of the study

The study site, called Forbonnet peatland, is a part of a larger peatland complex named the Frasne peatland. The Forbonnet peatland can be subdivided into a *Sphagnum* dominated bog to the S (bog, ~7 ha) and a fen dominated by vascular plants to the N (~1.4 ha, *sedge* and *Molinia caerulea*). Bog and fen are surrounded by topographically higher, wooded and more mature peatlands (Figs. 2 and 3) that constitute a 300-ha complex of varying evolution stages. Local patches of *Phragmites* on the contours of the bog are indicative for punctual minerotrophic conditions. Carbon-14 dating of peat material revealed an age of 7250 ± 60 years BP for the bottom of the mature and wooded peatland (Gauthier et al., 2019), and 910 ± 30 and 1530 ± 30 years BP respectively for the base of the southern and central bog areas (Goubet, 2015; unpublished data). These differences reflect the heterogeneous development of the peatland complex with patches of different degrees of maturity. The site is located in the upstream part of the Drugeon river catchment in the French Jura Mountains at 840 m asl (46.826°N, 6.1725°E, Fig. 1).

The study area is characterized by almost evenly distributed rainfall over the year ranging from 80 to 120 mm/month (Toussaint et al., 2020). In contrast, the monthly mean temperature is very variable from 0 °C in February to 15 °C in July with an annual average 7 °C for the monitoring period (2009–2020) according to our local observatory platform (Toussaint et al., 2020).

From a geological point of view, the site is located within the folded part or the Jura Mountains with SW-NE trending anticlines and synclines affecting mainly limestones and marls of the Upper Jurassic and Lower Cretaceous. Subsequent erosion shaped the topography and favored the formation of karstic landforms. Within the synclines the karstified limestones are partially overlain by impervious or semi-impervious Quaternary moraines of varying thickness (from a few cm to meters), favoring locally the occurrence of lakes and wetlands (e.g., lake of Saint-Point, lake of Joux, Fig. 1; Duraffourg and Palacio, 1981). Consistently, the Forbonnet peatland is located within an open syncline covered by heterogeneous moraines promoting water retention.

This particular geological and hydrometeorological context implies a complex hydrogeological functioning of the system. Within the peatland, the general water flow is oriented from south to north, with the fen next to the outlet at the northern limit of the site (Lhosmot et al., 2021). Since the restoration of a part of the site in 2015–2016 by backfilling of dewatering ditches and the construction of a dam (Calvar et al., 2018), the water table raised during 6 months from 20 to 55 cm in the southern part of the site but remained stable since then and varies today mainly in response to the hydrometeorological variability (; (Bertrand et al., 2021; Lhosmot et al., 2021)). Nevertheless, although water supply is mainly at least partly ensured by direct rainwater infiltration, concurrent inflows from the surrounding mature peatlands or from the underlying moraines have been suggested on the basis of geochemical indices (Collin, 2016; Lhosmot et al., 2021). In addition, local and regional geomorphological evidences such as karst springs and sinkholes, suggests punctual hydraulic connection with the underlying regional karst aquifer, which is recharged by groundwater flows from

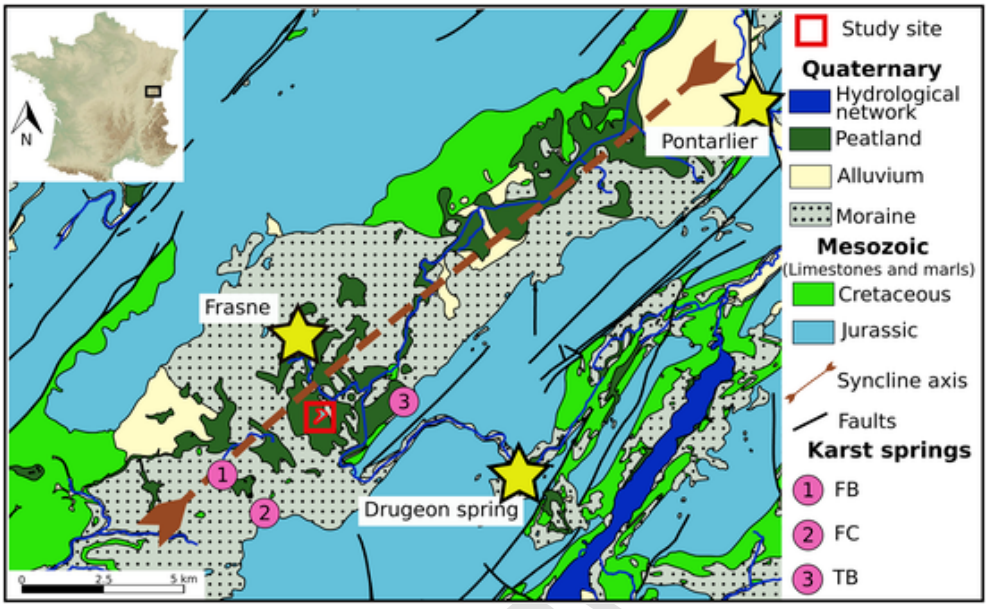

Fig. 1. Geological map (base map modified from BRGM) and site location (IGN France).

an adjacent anticline. Consistently, our previous study based on the ongoing hydrological and hydrochemical long-term monitoring at the outlet of the peatland allowed to distinguish the following water origins for the Forbonnet bog (Lhosmot et al., 2021; Fig. 2): 1) direct rainfall infiltrating the surface peat layer; 2) lateral seepage inputs from the neighboring raised wooded peatlands, sustaining the intermediate peat level; and 3) punctual karst water inputs at the substratum/peat interface supplying the deepest peat layer

2.1. Water sampling

The sampling strategy allowed to characterize both the acrotelm, e.g. the surface peat layer, and the catotelm, e.g. deep and intermediate peat layers in this study. The acrotelm is highly permeable and aerobic, and supports plant activities, whereas the catotelm is entirely waterlogged, which favors, together with its low permeability anaerobic conditions (Baird et al., 2016; Ingram, 1978). The study is based on two sampling campaigns during October 2019 (low flow) and February 2021 (high flow). This second campaign was originally planned for March 2020 but had to be postponed due to the Covid-19 lockdown.

The network of 19 piezometers follows the general upstream-downstream gradient (Fig. 3). Downstream, 2 piezometers (BM1 and BM3) are located within the fen, 1 piezometer (BM12) at the boundary between fen and bog, while the others are located upstream within the bog (Fig. 3). Among them, respectively nine and eleven piezometers were sampled in October 2019 and February 2021 (Fig. 3). Some of the piezometers (PP1–2-3, TV1–2-3, TV4–5-6) are nested panpipes, allowing the sampling of surface (TV3, TV6, PP3; depth < 0.5 m from peat surface), intermediate (TV2: 1.5 ± 0.3, TV5:1.2 ± 0.3, PP2: 0.9 ± 0.30 m) and deep (TV1: 2.27 ± 0.1, TV4: 2.35 ± 0.1, PP1: 1.7 ± 0.45 m) peat pore water. The panpipe arrays A-B and C—D enable sampling of intermediate (A and C, 1 ± 0.1 m) and deep (B and D, 1.85 and 2.6 ± 0.1 m) peat pore waters, close to the interface with the underlying geological substrate. These panpipe arrays allow to characterize separately the pore water of the fibric peat of the acrotelm and of the more mature peat of the underlying catotelm (intermediate/deep peat layers) (Lhosmot et al., 2021; Bertrand et al., 2021 and references therein). All other piezometers (BM1–3–12-18, GB, TV7–9-12) are fully screened and were sampled at the surface (< 0.5 m) and at different depths (~1 m for BM1 and 2 m for others piezometers) in February 2021, while only one integrative sample was taken in October 2019. All piezometer water samples were recovered with a peristaltic pump.

In order to characterize the system outflow, the main outlet (O_central) and its two tributaries (O_left and O_right, Figs. 1 and 2) were also sampled. O_right drains ~20% of the topographic catchment (total area

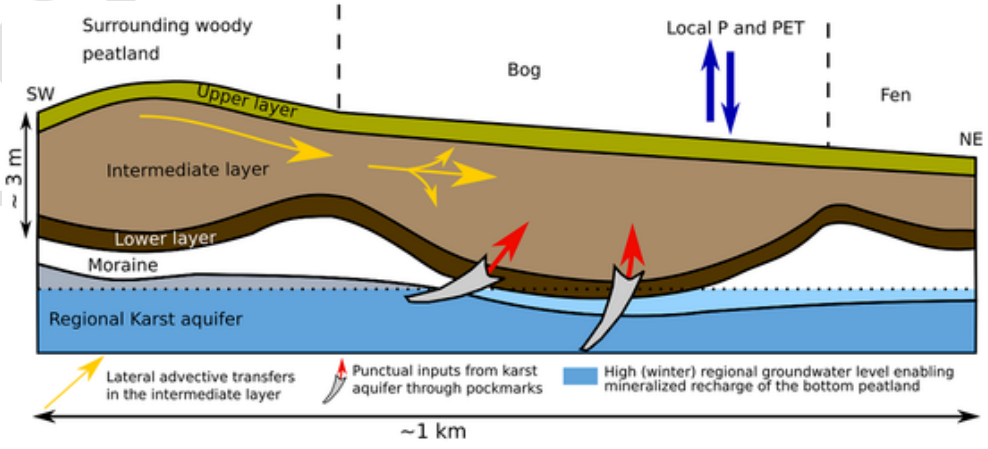

Fig. 2. Conceptual scheme of the hydrological context of the Frasne peatlands (after Lhosmot et al., 2021).

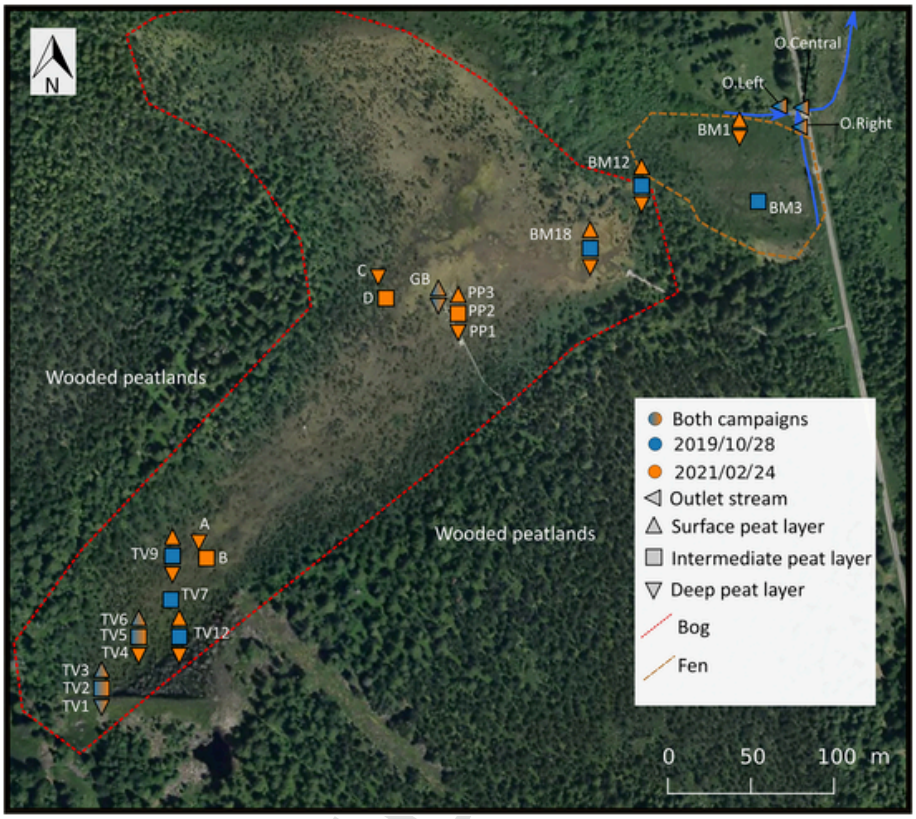

Fig. 3. Localization of sampling points over the Forbonnet peatland.

of 1 km² determined from digital elevation models) including the main part of the bog.

In parallel, 3 nearby karst springs (TB, FB, and FC) were sampled to characterize the regional karst aquifer. TB was sampled once in February 2021. It is located at the foot of the a nearby anticline, which presumably is the recharge zone of the aquifer beneath the study site (Fig. 3). The springs FB and FC are located within the syncline and are possibly not only fed by the karst aquifer, but also by local perched aquifers within the moraines. Springs FB and FC where sampled once in October 2019.

The waters samples were filtered (0.45 µm for major elements; 0.22 µm for DOC) within 12 h after sampling, while unfiltered aliquots were kept for carbon-13 analyses. We have rigorously ensured that aliquots for carbon-13 analyses did not contain air bubbles. Also, in order to minimize mineralization of organic matter, carbon-13 samples were analyzed within three weeks after sampling. The aliquots for cation analyses were acidified after filtering to pH 2 with ultrapure nitric acid. All samples were stored at 4 °C until analyzes, in glass aliquots for carbont-13 and HDPE tubes for other analyzes.

2.2. Dissolved carbon dioxide concentration in peat pore water

In order to evaluate the CO_2 exchange between the peatland and the atmosphere CO_2 concentrations were determined 6 times (27/04/2021; 27 and 28/05/2021; 22/06/2021; 20/07/2021 and 14/09/2021) at 3 different depths in the panpipe array system PP1–2-3 using a Pro Oceanus Mini Submersible pCO_2 sensor (Fig. 4).

2.3. Physico-chemical analyses

Electrical Conductivity (EC), Temperature (T) and pH were measured in the field with manual multimeters (ODEON Ponsel SN-ODE OA and WTW 340i).

Cation (Ca^{2+}, K^+, Na^+, Mg^{2+}, Sr^{2+}) and anion (Cl^-, SO_4^{2-}, NO_3^-) concentrations were determined respectively by ICP-AES (Thermo iCAP 6500) and HPLC (ICS 1000) at the PEA²t analytical platform of the Chrono-Environnement laboratory. The analytical error for ICP-AES is in average 4% and for HPLC is <5%. Total S was also measured by ICP AES. HCO_3^- concentrations were determined by Gran titration using 0.01 M sulfuric acid. Concentrations of the other DIC phases (H_2CO_3 and CO_3^{2-}) were calculated according to Langmuir (1997). In this study we focus mainly on HCO_3^- and Ca^{2+} concentrations because the electrical conductivity of peat pore water is essentially related to these ions (Lhosmot et al., 2021). All anion and cation concentrations were used to assess the accuracy of the measurement by calculating the Normalized Inorganic Charge Balance (NICB) and are available in the Supplementary Table S1.

NICB was well-balanced for the most mineralized waters (EC > 200 µS cm^{-1}, NICB = 2 ± 4.3%, n = 10). However, a relative cation excess was found in the least mineralized samples (EC < 50 µS cm^{-1}, NICB = 43.2 ± 25.3%, n = 21). This kind of unbalance is well known for peatland waters and generally attributed to the negative charge of DOC, which is not included in the calculation of the NICB (Reeve et al., 1996; Steinmann and Shotyk, 1997; Urban et al., 2011). The relative cation excess does therefore not query the analytical accuracy of the measurements

DOC was analyzed by catalytic combustion (Vario TOC cube, ± 0.5 mg/L) after purging of DIC by addition of hydrochloric acid.

2.4. Isotopic analyses

Carbon-13 signatures of DIC ($\delta^{13}C_{DIC}$) were analyzed using a mass spectrometer (Elementar Isoprime 100) coupled with an equilibration system (Elementar MultiFlow-Geo). Samples were acidified using phosphoric acid and flushed with helium. Standards included Na_2CO_3 and $NaHCO_3$ as well as internal water standards. Standards were systemati-

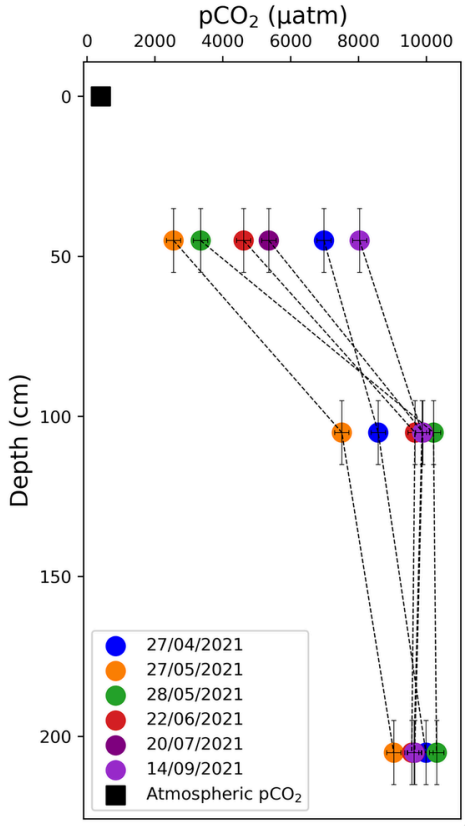

Fig. 4. Circles represent pCO_2 (ppm) measured in nested panpipes array (PP1–2-3) for 6 dates. The black square represents the atmospheric pCO_2. Horizontal uncertainty was calculated according to the probe manual.

cally analyzed after 8 samples to check measurement stability. All samples were analyzed twice.

The $\delta^{13}C_{DIC}$ signature was expressed versus the Pee Dee Belemnite (V-PDB) international standard and calculated according to Eq. (1).

$$\delta^{13}C_{DIC}\ (‰) = \left[\frac{\frac{^{13}C}{^{12}C\ sample}}{\frac{^{13}C}{^{12}C\ PDB}} - 1\right] \times 1000 \quad (1)$$

The analytic error was ±0.11 ‰.

2.5. Simulation of $\delta^{13}C_{DIC}$ signatures

In order to control the origin and the fractionation of DIC, the $\delta^{13}C_{DIC}$ signatures were modeled according to various hypotheses dealing with the concept of open and closed system to atmosphere defined by Garrels and Christ (1965) and Langmuir (1971). These models are based on the mixing balance of different carbon isotope end-members introduced by Deines et al. (1974).

Firstly, we hypothesized open conditions with respect to soil CO_2 and a pure biogenic origin for DIC (Eq. (2)).

$$\delta^{13}C_{DIC-open} = \frac{[H_2CO_3] * \left(\delta^{13}C_{biogenic} + \varepsilon_{CO_{2(g)}-H_2CO_3}\right) + \left[HCO_3^-\right] * \left(\right.}{\left[H_2CO\right.}$$

Where

$\delta^{13}C_{biogenic}$ is the $\delta^{13}C$ of C3 plants, as described below.

$\varepsilon_{CO_{2(g)}-H_2CO_3}$ is the fractionation factor from gaseous CO_2 to dissolved CO_2 (carbonic acid).

$\varepsilon_{CO_{2(g)}-HCO_3^-}$ is the fractionation factor from gaseous CO_2 to dissolved bicarbonate.

$\varepsilon_{CO_{2(g)}-CO_3^{2-}}$ is the fractionation factor from gaseous CO_2 to dissolved carbonate.

Secondly, by taking into account the regional hydrogeological context (Figs. 1 and 2), we considered that limestone dissolution may occur mainly under closed system conditions with respect to CO_2, as commonly observed in karst aquifer. In this context bicarbonates can be considered as an equimolar mixture of biogenic and carbonate carbon (Batiot-Guilhe, 2002; Emblanch et al., 1998; Gillon et al., 2009; Langmuir, 1997, Eq. (3)).

$$CaCO_3 + H_2CO_3 \rightarrow Ca^{2+} + 2HCO_3^{2-} \quad (3)$$

For such closed system conditions, the $\delta^{13}C_{DIC}$ signatures thus reflect for one half the biogenic signature of soil CO_2 and for the other half the calcite signature of limestone according to Eq. (4):

$$\delta^{13}C_{DIC-closed} = \frac{\left([H_2CO_3] + \frac{[HCO_3^-]}{2} + \frac{\left[CO_3^{2-}\right]}{2}\right) * \left(\delta^{13}C_{biogenic} + \varepsilon_{CO_{2(}\right.}{\left[H_2CO_3\right.}$$

With the same notations as for Eq. (2), but additionally with:

$\delta^{13}C_{CaCO_3}$ is $\delta^{13}C$ of carbonates mainly composed of calcite.

$\varepsilon_{CaCO_3-CO_3^{2-}}$ is the fractionation factor from calcite to dissolved carbonate ($\varepsilon_{CO_{(g)}-CO_3^{2-}} + \varepsilon_{CaCO_3-CO_{2(g)}}$).

The thermodependent enrichment factors (ε) were calculated by the empirical equations given in Table 1.

Applying these models requires to fix the $\delta^{13}C$ composition of the different DIC end-members. Colombié et al. (2011) and Joachimski (1994) found for limestones of the Jura Mountains $\delta^{13}C$ range from −5 to +3 ‰ V-PDB. Accordingly, we set $\delta^{13}C_{CaCO3}$ to 0 ‰ V-PDB and used the range of −5 - +3 ‰ as confidence interval.

The syncline structure of the watershed is exclusively covered by C3 plants, as for temperate regions (Still et al., 2003). The vegetation cover is marked by an alternance of temperate forests, wetlands and pastures. The area is too high for the cultivation of C4 plants (corn) (NGHIEM, 2006). For C3 plant dominated areas, the initial $\delta^{13}C$ signature of soil organic matter ranges from −30 to −25 ‰ (Buzek et al., 2019; Delarue et al., 2011; Loisel et al., 2010), followed by a shift of up to 4.4 ‰ during the subsequent aerobic decomposition of soil organic matter and diffusion of CO_2 (Cerling et al., 1991). Consequently, $\delta^{13}C_{CO2}$ was set to −21 and − 22 ‰ V-PDB for aerobic forest soils in temperate mid-mountain covered by C3 plant (Bertrand et al., 2013; Emblanch et al., 2003). However, CO_2 diffusion is limited in water-logged soils, leading to a weaker positive shift during decomposition of organic matter (Neumann et al., 2016; Preuss et al., 2012). In agreement with this a $\delta^{13}C$ of −28 to −26 ‰ was found for the organic matter of the Forbonnet bog in a previous study (Delarue et al., 2011). Consequently, we

Table 1
Enrichment factors (in ‰).

Fractionation factor	Equation	Reference
$\varepsilon\ ^{13}C_{CO2(g)\text{-}H2CO23aq}$	$10^3 \ln\alpha\ ^{13}C_{CO2(g)\text{-}H2CO3(aq)} = -0.373\ (10^3\ T^{-1}) + 0.19$	(Vogel et al., 1970)
$\varepsilon\ ^{13}C_{CO2(g)\text{-}HCO3}$	$10^3 \ln\alpha^{13}C_{CO2(g)\text{-}HCO3} = 9.552\ (10^3\ T^{-1}) - 24.10$	(Mook et al., 1974)
$\varepsilon\ ^{13}C_{CO2(g)\text{-}CO3}$	$10^3 \ln\alpha^{13}C_{CO2(g)\text{-}CO3} = 0.87\ (10^6\ T^{-2}) - 3.4$	(Deines et al., 1974)
$\varepsilon\ ^{13}C_{CaCO3\text{-}CO2(g)}$ -	$10^3 \ln\alpha^{13}C_{CaCO3\text{-}CO2(g)} = -2.988\ (10^6\ T^{-2}) + 7.6663\ (10^3\ T^{-1}) - 24{,}642$	(Bottinga, 1968)

used for modeling a wide range of $\delta^{13}C_{biogenic}$ of-24.5 ± 3.5 ‰ in order to account at once for limited and important CO_2 diffusion.

The $\delta^{13}C_{DIC}$ signature could be modeled for most samples except for those with bicarbonate concentrations below the detection limit of 5 mg/L. These samples correspond to superficial bog waters from specific rainfall dominated zone (Fig. 3, BM18 for October 2019 and Feb. 2021, BM12, GB_{surf} and PP3 for Feb. 2021, mean EC = 31.3 µS cm^{-1}).

Closed system simulation (Eq. (4)) was used for the karst spring samples and the intermediate and deep pore water samples, whereas open system simulation (Eq. (2)) was applied for the outlet samples and the surface peat pore water samples.

In order to compare the simulations modeled and measured $\delta^{13}C_{DIC}$ compositions, we defined $\Delta\delta^{13}C_{DIC}$ reflecting the offset between measured and modeled $\delta^{13}C_{DIC}$ (Eq. (5)):

$$\Delta\delta^{13}C_{DIC} = \text{Measured } \delta^{13}C_{DIC} - \text{Calculated } \delta^{13}C_{DIC} \quad (5)$$

A $\Delta\delta^{13}C_{DIC}$ value of zero suggests that the model describes satisfactorily the end-members and mechanisms of DIC formation. In contrast, non-zero values of $\Delta\delta^{13}C_{DIC}$ imply the existence of end-members and mechanisms not considered by the model.

3. Results

3.1. Water physico-chemical properties and spatio-temporal variability

The complete analytical results of the two sampling campaigns are available in Table S1 of the Supplementary material. Analytic uncertainties given within the manuscript correspond to standard deviation. Redox and sulfate concentration are only available for the February campaign.

The partial CO_2 pressure (pCO_2) measured in the central panpipe array (piezometers PP1–2-3, Figs. 4, 6 measurement dates) was systematically lower in the surface peat layer (PP3, 5144 ± 2099 ppm; Fig. 4) than in the deeper catotelmic layer (intermediate and deep, PP1 and 2, 9287 ± 1036 and 9696 ± 425 ppm). In addition, we observed a seasonal trend (especially in surface, e.g., PP3 piezometer) with an increase of pCO_2 from May to September excepted for 27/04/2021 which corresponded to an outstanding dry and warm period.

The peat pore water temperature showed no depth gradient in October 2019, but homogeneous values between 10 and 11.8 °C. In contrast, in February 2021 the temperature increased from 1.9 °C in the surface layer to 6.8 °C in the deep peat layers, showing the thermal inertia of peat (McKenzie et al., 2007). All other parameters were similar for both campaigns and are therefore presented together.

The EC covered a large range from 9.2 to 820 µS cm^{-1} with a mean of 160 µS cm^{-1}. EC was strongly positively correlated with bicarbonate (R^2 = 0.96, pvalue ≤ 0.005, n = 47) and calcium concentrations (R^2 = 0.98, pvalue <0.005), showing that EC essentially reflects the calcite dissolution typical for karst systems (Jeannin et al., 2016; Lhosmot et al., 2021).

The bog's surface water was poorly mineralized and acid (pH 4 to 5 and EC < 100 µS cm^{-1}), whereas the deep peat pore waters were more mineralized and less acid (pH 5.5 to 6.6 and EC > 100 µS cm^{-1}). However, some deep peat waters were only poorly mineralized (EC < 100 µS cm^{-1}; Fig. 5). The redox potential showed a similar vertical gradient with well oxygenated conditions near the surface (301 mV) and reducing conditions at depth (13.3 mV) with a mean of 168 mV.

The DIC speciation calculations showed that DIC of the peat pore waters was entirely composed of H_2CO_3 and HCO_3^-, whereas CO_3^{2-} was absent due to the relatively acid pH (Langmuir, 1997). The strongly mineralized bog waters (EC > 100 µS cm^{-1}, mean = 375 µS cm^{-1}, n = 12) had concomitantly high HCO_3^- (mean = 3.8 ± 2.5 mmol/L) and H_2CO_3 concentrations (mean = 5.7 ± 3.4 mmol/L). The poorly mineralized bog waters (EC < 100 µS cm^{-1}, mean = 40 µS cm^{-1}, n = 16) showed lower HCO_3^- (mean = 0.28 ± 0.2 mmol/L) and higher H_2CO_3 concentrations (mean = 9 ± 10 mmol/L). The downstream waters in the fen and at the outlet (n = 9) had low concentrations of HCO_3^- (mean = 0.55 ± 0.25 mmol/L) and H_2CO_3 (mean = 0.7 ± 0.8 mmol/L). At least, the karst waters (pH = 7.2 ± 0.3, n = 3) showed high HCO_3^- (4.9 ± 1 mmol/L), low H_2CO_3 (1.1 ± 0.9 mmol/L) and very low CO_3^{2-} (0.003 ± 0.001 mmol/L) concentrations.

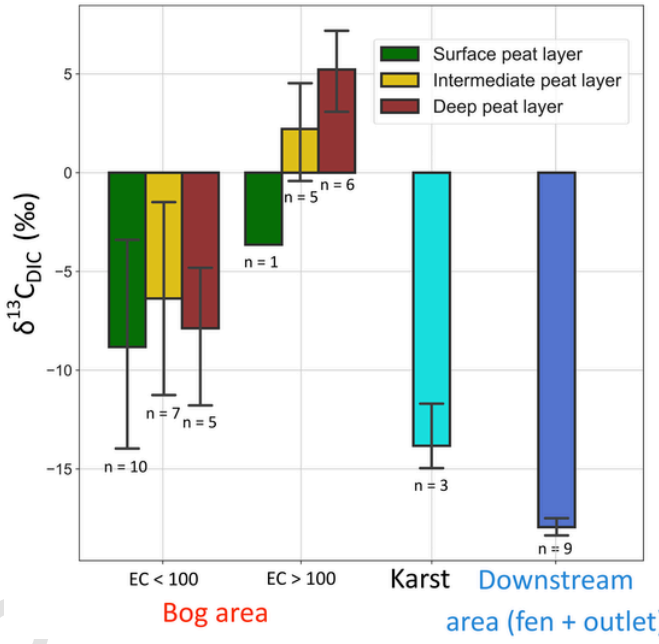

Fig. 5. Barplot showing $\delta^{13}C_{DIC}$ distribution according to water types. Error bars represent the standard deviation.

The sulfate concentrations were low in the bog (mean = 1 ± 5 µmol/L) and significantly higher (pvalue = 0.046) in the downstream area and the karst water samples (16 ± 22 µmol/L). However, despite bog pore water showed very low sulfate concentrations, elementary Sulfur (S) was found in these waters (mean = 16 ± 12 µmol/L).

The DOC concentrations of the peatland waters varied from 19.5 to 62.2 mg/L with a mean of 37.2 mg/L (raw data in the Table S1). The lowest values (pvalue <0.005, n = 34) occurred in the deep layer (24.5 mg/L) and the values were higher in the intermediate (38.8 mg/L) and surface (35.4 mg/L) layers. The DOC concentrations of the karst springs were much lower (2.8 ± 0.8 mg/L, n = 3).

3.2. $\delta^{13}C_{DIC}$ signatures

The $\delta^{13}C_{DIC}$ were heterogeneous over the peatland and varied between −22.0 and + 8.1‰ V-PDB (Fig. 5). At first sight, these signatures are within the range of the 3 potential end-members, i.e. geogenic (carbonated minerals), biogenic (issued from C3 vegetation and soil respiration) and atmospheric CO_2 (−8.4 ‰; Campeau et al., 2017; Graven et al., 2020). The $\delta^{13}C_{DIC}$ composition of regional karst water was characterized by intermediate values (Fig. 5; −11.7 ‰ for spring TB in February 2021, −15.0 and − 14.9 ‰ for springs FB and FC in October 2019). Similar values than TB spring were found by Emblanch et al. (2003) for karst springs in southern France (−11 to 13 ‰,) and by Celle-Jeanton et al. (2003) for karst springs of the Jura Mountains (−9 to −14 ‰). The values for FB and FC spring were lower than Emblanch et al. (2003) (2 ‰) and Celle-Jeanton et al. (2003) (1 ‰) but remain in the similar range.

The heterogeneous spatial distribution of the $\delta^{13}C_{DIC}$ values of the bog water samples were related to EC and depth gradients (Fig. 5). Poorly mineralized samples (EC < 100 µS cm^{-1}, mean = 40 µS cm^{-1},

$\delta^{13}C_{DIC}$ = −7.8 ± 7 ‰, n = 22) had lower $\delta^{13}C_{DIC}$ than more mineralized ones (EC > 100 µS cm^{-1}, mean = 375 µS cm^{-1}, $\delta^{13}C_{DIC}$ = 3.2 ± 3.8 ‰, n = 12, pvalue = 0.32). The $\delta^{13}C_{DIC}$ composition of the surface samples was generally more negative ($\delta^{13}C_{DIC}$ = −8.3 ± 8.3 ‰) than for the catotelmic waters (intermediate and deep layers; $\delta^{13}C_{DIC}$ = −2 ± 7.3 ‰, Fig. 5). This vertical gradient was observable for both poorly and highly mineralized waters (Fig. 5).

From an ecohydrological perspective, the $\delta^{13}C_{DIC}$ was below −16.6 ‰ in the downstream area (fen and outlet, median = −18.2 ‰) while the median for the bog pore water was −7.5 ‰ (Fig. 5). Only a few samples from within the bog showed more depleted $\delta^{13}C_{DIC}$: $BM12_{surf}$ and $BM12_{deep}$ (−22 and − 17.1 ‰, February 2021) localized at the boundary between the bog and the fen; PP3 (−20 ‰, Feb.2021) and TV9 (−17.9 ‰, October 2019). In addition, it is worth noting that $\delta^{13}C_{DIC}$ of the downstream area (fen and outlet) were depleted for all water types (stream, surface and deep peat pore water), suggesting that the vertical gradient observed within the bog disappeared in the downstream area.

3.3. Measured vs modeled $\delta^{13}C_{DIC}$

The mean $\Delta\delta^{13}C_{DIC}$ of 3.3 ± 1.6 ‰ of the karst springs is close to zero and intersect the 1:1 line when considering the confidence interval, i.e. in agreement with the hypothesis of an equimolar mixture of biogenic and geogenic carbon (Fig. 6-A-B). Within the peatland, the $\Delta\delta^{13}C_{DIC}$ is similarly close to zero for the downstream samples (fen and outlet, $\Delta\delta^{13}C_{DIC}$ of 0.8 ± 3 ‰ and 1.3 ± 3 ‰ respectively, Fig. 6-A). In contrast, the bog pore waters were systematically offset from the 1:1 line with strongly positive $\Delta\delta^{13}C_{DIC}$ of 21.9 ± 5 ‰ (Fig. 6).

4. Discussion

Lhosmot et al. (2021) delineated 3 water origins, direct rainfall, lateral from the peatland complex, and mineralized groundwater. The meteoric and lateral waters may be purveyors of biogenic DIC thanks to equilibrium with soil CO_2 respiration while groundwater brings both biogenic and geogenic DIC. Accordingly, we can make the hypothesis (1) that autochthonous DIC from mineralization of organic matter represents almost 100% of DIC in the upper peat layer and (2) that allochthonous DIC from limestone weathering represents almost 100% of DIC. Intermediate fractions of autochthonous and allochthonous DIC result from mixing between these two end-members. However, as it will be discussed in the following, further speciation processes affecting the final carbon-13 signatures of DIC avoid to directly quantify the proportion of each DIC source. Radiocarbon should help to bring a such quantification (Chasar et al., 2000).

In order to improve the understanding of this complex system combining different water and carbon origins and DIC fractionation, we organized the continuation of the discussion in 3 Sections: (1) the atmospheric pattern; (2) the hydrogeological gradient, which take into account the influence of calcareous DIC and (3) the ecohydrological contrasts between the bog and the fen.

4.1. Atmospheric constraints over DIC patterns

The vertical pCO_2 profiles show that the partial pressure in the surface peat layer is between 5 and 20 times higher than in the atmosphere (Fig. 4). This supports the hypothesis of CO_2 outgassing to the atmosphere. This process is commonly observed for stream waters and usually leads to enriched $\delta^{13}C_{DIC}$ values (Abril et al., 2014; Luo et al., 2019), which is even accentuated by partial equilibration with atmospheric CO_2 (+8 ‰). The duration of water-atmosphere exchange is an additional parameter controlling CO_2 outgassing, making the degree of fractionation due to outgassing qualitatively observable, but remains, however, difficult to quantify (Deirmendjian and Abril, 2018). In the context of the Forbonnet peatland, pCO_2 are almost identical in the intermediate and deep catotelm layers, suggesting that CO_2 outgassing is limited to the acrotelm (Fig. 4).

4.2. Hydrogeological constraints for DIC speciation

The important and systematically positive $\Delta\delta^{13}C_{DIC}$ values of the deep catotelm layer could result from methane production, broadly observed in peatlands and resulting in an isotopic enrichment of $\delta^{13}C_{DIC}$ (Campeau et al., 2018; Corbett et al., 2013; Galand et al., 2010; Holmes et al., 2015; Lansdown et al., 1992; Steinmann et al., 2008). Such a process is in agreement with the methane fluxes observed at the Forbonnet peatland during the period of field sampling (Jacotot et al. 2021; Lhosmot et al., 2022). Consistently, the highly positive $\Delta\delta^{13}C_{DIC}$ values of the catotelmic bog samples exclude an atmospheric influence. The values are furthermore negatively correlated with redox

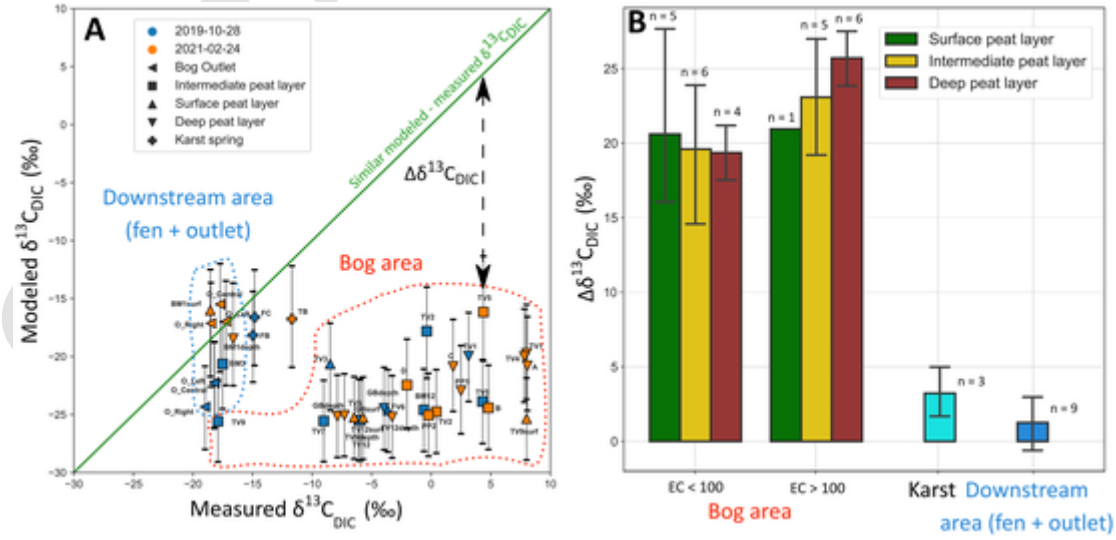

Fig. 6. A: Calculated vs measured $\delta^{13}C_{DIC}$. The 1:1 line correspond to similar modeled and measured values. The vertical error corresponds to the range of simulated $\delta^{13}C_{DIC}$ using range of confidence for source material ($\delta^{13}C_{biogenic}$ and $\delta^{13}C_{CaCO3}$) described in "Simulation of $\delta^{13}C_{DIC}$ signatures" paragraph.
B: Barplot showing $\Delta\delta^{13}C_{DIC}$ distribution according to water types. $\Delta\delta^{13}C_{DIC}$ is the difference between the modeled and the measured $\delta^{13}C_{DIC}$ (Eq.8). Error bars represent the standard deviation.

(R^2 = 0.44, pvalue <0.05), suggesting that biologically-mediated processes such as reduction might occur (Fig. 7-A).

Methanogenesis generally occurs only after complete sulfate reduction (Andersen et al., 2013; Gauci et al., 2002; Koebsch et al., 2019; Reddy and DeLaune, 2008). Consistently, the bog waters showed very low sulfate concentrations suggesting that S was fixed within the bog in reduced form (Eq. (6)), favoring the activity of methanogens.

$$SO_4^{2-} + 2CH_2O = 2HCO_3 + H_2S \quad (6)$$

When plotting $\Delta\delta^{13}C_{DIC}$ versus pH a peak of $\Delta\delta^{13}C_{DIC}$ around pH 6 is observed (Fig. 7-B), similar to the results of Sizova et al. (2003). Although there is no general consensus regarding pH effects on methane production (Conrad, 2020), Dunfield et al. (1993) showed that methane production is stronger for neutral than for acidic pH. In this study, the pH range around 6 is due to the presence of bicarbonate-rich waters, which are preferentially found at the bottom of the bog close to the contact with the geological substratum (Lhosmot et al., 2021). Consistently, Bräuer et al. (2004) found in an experimental study that the addition of H_2/CO_2 stimulated methanogenesis in a circumneutral pH fen whereas the effect was limited under acidic conditions.

Nevertheless, the relation between $\Delta\delta^{13}C_{DIC}$ and the groundwater markers Ca^{2+}, HCO_3^-, EC is more complex (Figs. 7-C, E, and F). For low concentrations (Ca^{2+}: < 75 mg/L, HCO_3^-: < 100 mg/L; Mg^{2+}: < 1 mg/L and EC < 200 µS cm^{-1}) $\Delta\delta^{13}C_{DIC}$ increased with a steep slope with increasing concentrations of groundwater markers until reaching a threshold (Fig. 7-C, E, and F). Beyond this threshold, the slope disappeared, consistently with the laboratory data of Lamers et al. (1999), who showed that up to a threshold of 1 mmol/L (or 61 mg/L) increasing bicarbonate concentrations significantly amplify methanogenesis, which is in perfect agreement with the $\Delta\delta^{13}C_{DIC}$ - HCO_3^- relationship of our data (Fig. 7-C).

These relationships suggest that reduced conditions, combined with pH buffering and bicarbonate fluxes, modify $\delta^{13}C_{DIC}$ in the deeper peat layer through methane production (Fig. 8). In this perspective, the observed link between high $\Delta\delta^{13}C_{DIC}$ and low DOC could be related to groundwater inputs with high HCO_3^- and low DOC concentrations, which lead to high $\Delta\delta^{13}C_{DIC}$ by methanogenesis and low DOC concentrations by dilution (Fig. 7-D). This specific chemistry is suspected to be linked to punctual groundwater inputs at the bottom of the bog (Fig. 2) suggested by Lhosmot et al. (2021).

Methanogenesis is essentially based on 2 main metabolic pathways, acetoclastic methanogenesis (AM, Eq. (7)) and hydrogenotrophic methanogenesis (HM, Eqs. (8–10)). Their relative contributions may vary from 0 to 100% depending on the one hand on the type of substrate and on the other hand on microbial, physico-chemical and seasonal conditions (Conrad, 2020; Xu et al., 2015; Throckmorton et al., 2015).

$$CH_3COOH = CH_4 + CO_2 \quad (7)$$
$$2CH_2O + 2H_2O = 2CO_2 + 4H_2 \quad (8)$$
$$CO_2 + 4H_2 = CH_4 + 2H_2O \quad (9)$$
$$2CH_2O = CH_4 + CO_2 \quad (10)$$

Both AM and HM produce methane and carbon dioxide in equal proportions (Corbett et al., 2013; Neumann et al., 2016).

According to the geochemical reactions discussed above, bicarbonate of karstic origin could be an electron acceptor to favor HM (Eq. (9)), especially in the catotelm with more mineralized pore waters. This pathway could be predominant as suggested by Hornibrook et al. (1997) and Lansdown et al. (1992), who showed in a temperate bog that methane production was entirely related to HM. Chasar et al. (2000) furthermore demonstrated a northern Minnesota peatland by ra-

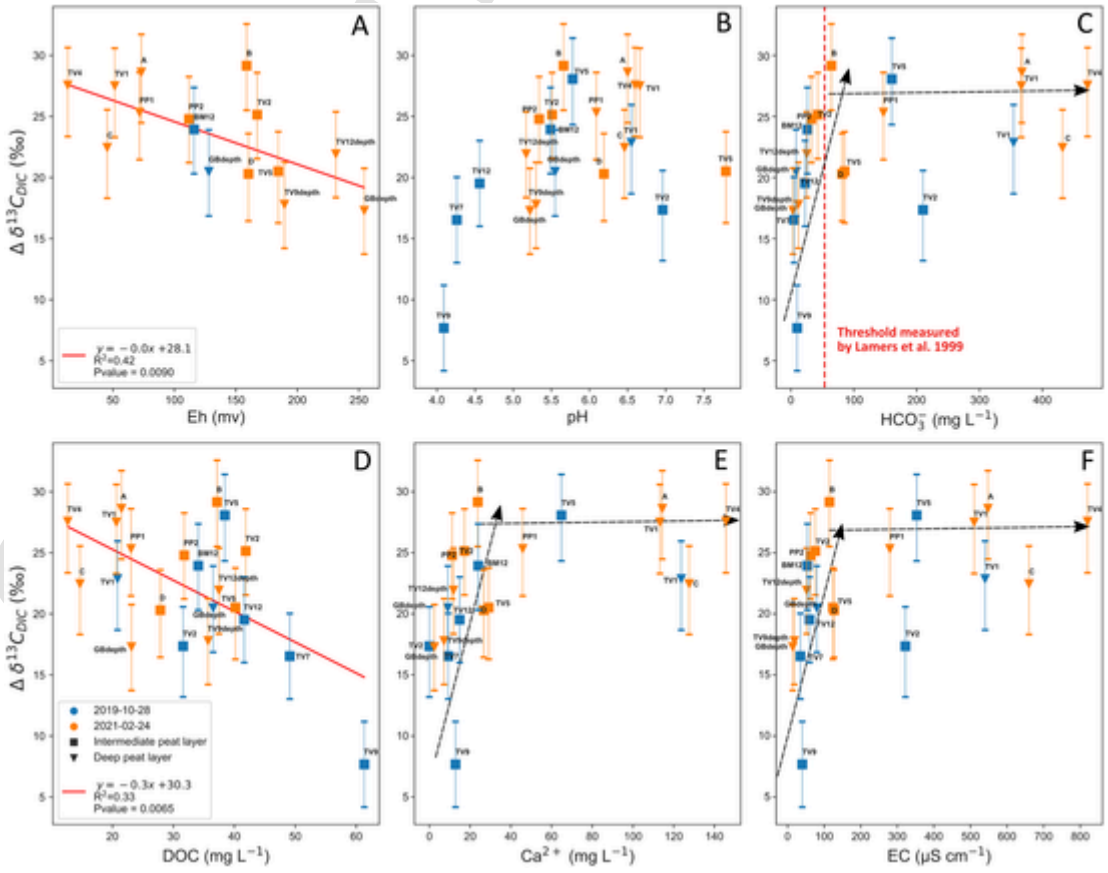

Fig. 7. $\Delta\delta^{13}C_{DIC}$ function of water physico-chemical parameters for catotelmic (intermediate and deep) bog porewater.

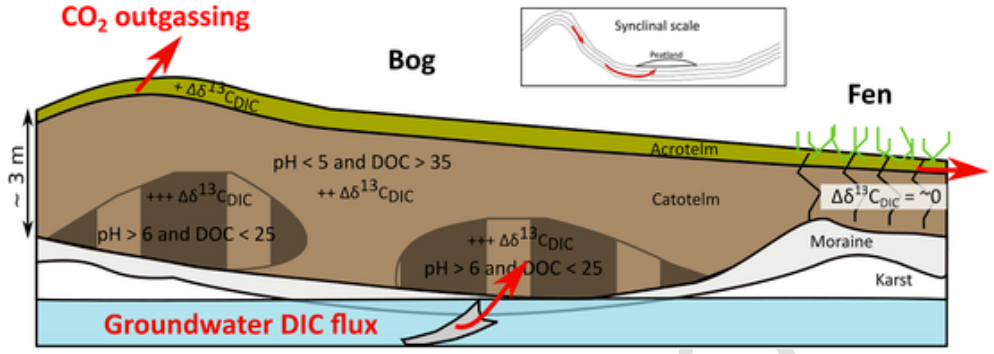

Fig. 8. Conceptual scheme of processes fractioning $\delta^{13}C_{DIC}$ along the vertical and ecological (fen-bog) gradients at the Forbonnet peatland. The red arrows represent DIC fluxes between the peatland and other DIC compartments. (For interpretation of the references to colour in this figure legend, the reader is referred to the web version of this article.)

diocarbon tracing that DIC from groundwater recharge was used for methane production.

4.3. Ecohydrological constraints for $\delta^{13}C_{DIC}$ fractionation

At the ecosystem scale, the contrasting DIC concentrations and $\delta^{13}C_{DIC}$ compositions between bog and fen argue for an ecohydrological constraint for DIC speciation. From the upstream (bog)-downstream (fen) gradient perspective, the limited ^{13}C enrichment in the fen ($\Delta\delta^{13}C_{DIC}$ 0.8 ± 3 ‰) compared to the anaerobic bog ($\Delta\delta^{13}C_{DIC}$ 22.2 ± 5.2 ‰) could be attributed to the mechanisms described below:

First, methane production could simply be limited within the fen. This hypothesis is strengthened by the sulfate concentrations, which are higher than in the bog. Consistently, Alstad and Whiticar (2011) reported lower CH_4 pore water concentrations in the fen than in the bog of a Canadian peatland. Corbett et al. (2013) stated that fens contained more labile organic matter to support fermentation and higher rates of aerobic respiration due to oxygenation of the submerged soils by *Carex* roots. This non-fractionating pathway of organic matter production would lead to a depletion of $\delta^{13}C_{DIC}$ and should dominate the $\delta^{13}C_{DIC}$ signature (Campeau et al., 2017; Throckmorton et al., 2015).

Secondly, the AM pathway could be dominant in the fen as observed by Alstad and Whiticar (2011) or Galand et al. (2010). In fact, $\delta^{13}C_{DIC}$ is less fractionated by AM than by HM (Galand et al., 2010; Holmes et al., 2015; Whiticar et al., 1986).

These ecological constraints are potentially amplified by the thickness of the peat layers. In our case the fen is much shallower (mean of 114 cm, 97 manual measures) than the bog (mean of 196 cm, 298 manual measures; Collin, 2016), meaning that the catotelm (where methane is produced) is much thinner in the fen. This depth difference will also lead to a longer residence time of water in the catotelm of the bog, on the one hand because of the bigger volume and on the other hand because the compaction of the peat is stronger and consequently its hydraulic conductivity lower (Ingram, 1982).

5. Conclusions

This study shows that a mid-latitude mountainous peatland located on top of a karst aquifer is characterized by a wide panel of sources and processes affecting DIC. This work allows to delineate a conceptual typology showing that (1) CO_2 outgassing in the surface peat layer leads to a DIC flux to the atmosphere; (2) the calcareous water inflow, by rising the pH and the bicarbonate concentration in the deep catotelm layers, may favor methanogenesis that induces an enrichment of the $\delta^{13}C_{DIC}$; (3) the fen shows no enrichment of the $\delta^{13}C_{DIC}$ highlighting an ecohydrological (fen-bog) influenced by hydrological water residence time, sulfate concentrations and/or the predominance of different methanogenesis metabolic pathways.

In particular, the DIC fluxes in the acrotelm by CO_2 outgassing and the DIC-induced methanogenesis in the deep catotelm layers have to be quantified in future studies in order to evaluate their impact on the carbon budget of the peatland and the associated catchment basin. A particular attention has to be drawn on the sensitivity of these mechanisms to changing climate and on the existence of potential feedback loops. Therefore, it remains essential to pursue peatland monitoring over the long-term and to integrate groundwater-peatland interactions in the future monitoring setup.

Data availability statement

Physical and chemical parameters (T, EC, pH, eH, Ca^{2+}, SO_4^{2-}, Mg^{2+}, DOC, DIC, $\delta^{13}C_{DIC\text{-measured}}$, $\delta^{13}C_{DIC\text{-modeled}}$) measured on samples are available in the supporting information of this article. Further information is available on request to the corresponding author. Further information concerning the hydrological functioning of the Frasne peatland is available at doi: https://doi.org/10.1002/eco.2315 and doi: https://doi.org/10.1016/j.scitotenv.2020.141931.

Uncited reference

Declaration of Competing Interest

The authors declare that they have no known competing financial interests or personal relationships that could have appeared to influence the work reported in this paper.

Acknowledgements

The authors warmly thank the managers of the Regional Natural Reserve of Frasne-Bouverans for site access. This study was funded by the Bourgogne Franche-Comté Region (CRITICAL PEAT project, Acceuil de Nouvelle Equipe de Recherche Agreement n°2019-Y09069), the DIC Tracing project (SNO Tourbières). It was furthermore supported by the OSU THETA observatory of the university of Bourgogne Franche-Comté, the SNO Tourbières (https://www.sno-tourbieres.cnrs.fr/) and the French Network of Critical Zone Observatories (OZCAR) Network (https://wwwozca r-ri.org/fr/ozcar-observatoires-de-la-zone-critique-applicationset-recherche/). The SNO Tourbières observatory network was set up thanks to an incentive funding of the French Ministry of Research that allowed pooling together various pre-existing small-scale observation set-ups. The continuity of the field monitoring was made possible by a continuous CNRS-INSU funding since 2008. A. Lhosmot benefits from a Ph.D. fellowship of the French Ministry of Research. The authors would like to thank N. Crini and C. Amiot from the PEA2T analytical platform of the Chrono-Environnement laboratory for chemical analyses, and Lucy Gere and Issam Moussa, from the stable isotope fa-

cility of the Laboratoire d'ecologie Fonctionnelle et Environnement, Toulouse for $\delta^{13}C_{DIC}$ analysis. The authors also thank M. Nourdin for her contribution during field work. The authors thanks Christophe Emblanch and one anonymous reviewers for their constructive feedbacks allowing significant improvements of the final manuscript.

Appendix A. Supplementary data

Supplementary data to this article can be found online at https://doi.org/10.1016/j.chemgeo.2022.121254.

References

Abril, G., Martinez, J.-M., Artigas, L.F., Moreira-Turcq, P., Benedetti, M.F., Vidal, L., Meziane, T., Kim, J.-H., Bernardes, M.C., Savoye, N., Deborde, J., Souza, E.L., Albéric, P., Landim de Souza, M.F., Roland, F., 2014. Amazon River carbon dioxide outgassing fuelled by wetlands. Nature 505, 395–398. https://doi.org/10.1038/nature12797.

Alstad, K.P., Whiticar, M.J., 2011. Carbon and hydrogen isotope ratio characterization of methane dynamics for Fluxnet Peatland Ecosystems. Org. Geochem. 42, 548–558. https://doi.org/10.1016/j.orggeochem.2011.03.004.

Andersen, R., Chapman, S.J., Artz, R.R.E., 2013. Microbial communities in natural and disturbed peatlands: a review. Soil Biol. Biochem. 57, 979–994. https://doi.org/10.1016/j.soilbio.2012.10.003.

Anderson, S.P., Blum, J., Brantley, S.L., Chadwick, O., Chorover, J., Derry, L.A., Drever, J.I., Hering, J.G., Kirchner, J.W., Kump, L.R., Richter, D., White, A.E., 2004. Proposed initiative would study Earth's weathering engine. Eos Trans. AGU 85, 265. https://doi.org/10.1029/2004EO280001.

Baird, A.J., Milner, A.M., Blundell, A., Swindles, G.T., Morris, P.J., 2016. Microform-scale variations in peatland permeability and their ecohydrological implications. J. Ecol. 104, 531–544. https://doi.org/10.1111/1365-2745.12530.

Batiot-Guilhe, C., 2002. Étude expérimentale du cycle du carbone en régions karstiques : apport du carbone organique et du carbone minéral à la connaissance hydrogéologique des systèmes : site expérimental de Vaucluse, Jura, Larzac, région montpelliéraine, Nerja (Espagne) (These de doctorat). (Avignon).

Bernard-Jannin, L., Binet, S., Gogo, S., Leroy, F., Défarge, C., Jozja, N., Zocatelli, R., Perdereau, L., Laggoun-Défarge, F., 2018. Hydrological control of dissolved organic carbon dynamics in a rehabilitated *Sphagnum* -dominated peatland: a water-table based modelling approach. Hydrol. Earth Syst. Sci. 22, 4907–4920. https://doi.org/10.5194/hess-22-4907-2018.

Bertrand, G., Celle-Jeanton, H., Loock, S., Huneau, F., Lavastre, V., 2013. Contribution of PCO2eq and 13CTDIC evaluation to the identification of CO2 sources in volcanic groundwater systems: Influence of hydrometeorological conditions and lava flow morphologies—application to the Argnat basin (Chaîne des Puys, Massif Central, France). Aquat. Geochem. 19, 147–171. https://doi.org/10.1007/s10498-012-9185-0.

Bertrand, Guillaume, Ponçot, Alex, Pohl, Benjamin, Lhosmot, Alexandre, Steinmann, Marc, Johannet, Anne, Pinel, Sébastien, Caldirak, Huseyin, Artigue, Guillaume, Binet, Philippe, Bertrand, Catherine, Collin, Louis, Magnon, Geneviève, Gilbert, Daniel, Laggoun-Deffarge, Fatima, Toussaint, Marie-Laure, 2021. Statistical hydrology for evaluating peatland water table sensitivity to simple environmental variables and climate changes application to the mid-latitude/altitude Frasne peatland (Jura Mountains, France). Science of The Total Environment 754. https://doi.org/10.1016/j.scitotenv.2020.141931.

Billett, M.F., Garnett, M.H., Dinsmore, K.J., 2014. Should aquatic CO2 evasion be included in contemporary carbon budgets for peatland ecosystems? Ecosystems 18, 471–480. https://doi.org/10.1007/s10021-014-9838-5.

Bottinga, Y., 1968. Calculation of fractionation factors for carbon and oxygen isotopic exchange in the system calcite-carbon dioxide-water. J. Phys. Chem. 72, 800–808. https://doi.org/10.1021/j100849a008.

Bourbonniere, R.A., 2009. Review of water chemistry research in natural and disturbed peatlands. Canadian Water Res. J. 34, 393–414. https://doi.org/10.4296/cwrj3404393.

Bräuer, S.L., Yavitt, J.B., Zinder, S.H., 2004. Methanogenesis in McLean Bog, an acidic peat bog in upstate New York: stimulation by H2/CO2 in the presence of Rifampicinä, or by low concentrations of acetate. Geomicrobiol J. 21, 433–443. https://doi.org/10.1080/01490450490505400.

Buzek, F., Novak, M., Cejkova, B., Jackova, I., Curik, J., Veselovsky, F., Stepanova, M., Prechova, E., Bohdalkova, L., 2019. Assessing DOC export from a *Sphagnum* -dominated peatland using δ^{13}C and δ^{18}O–H_2O stable isotopes. In: Hydrological Processes hyp.13528. https://doi.org/10.1002/hyp.13528.

Calmels, D., Gaillardet, J., François, L., 2014. Sensitivity of carbonate weathering to soil CO2 production by biological activity along a temperate climate transect. Chem. Geol. 390, 74–86. https://doi.org/10.1016/j.chemgeo.2014.10.010.

Calvar, E., Moncorge, S., Bettinelli, L., Durlet, P., Magnon, G., 2018. Program LIFE+ "Bogs of the Jura": 60 bogs to restore in six years. In: Inventory, Value and Restoration of Peatlands and Mires: Recent Contributions. Hazi Foundation, pp. P108–P1133.

Campeau, A., Wallin, M.B., Giesler, R., Löfgren, S., Mörth, C.-M., Schiff, S., Venkiteswaran, J.J., Bishop, K., 2017. Multiple sources and sinks of dissolved inorganic carbon across Swedish streams, refocusing the lens of stable C isotopes. Nature 7, 9158. https://doi.org/10.1038/s41598-017-09049-9.

Campeau, A., Bishop, K., Nilsson, M.B., Klemedtsson, L., Laudon, H., Leith, F.I., Öquist, M., Wallin, M.B., 2018. Stable carbon isotopes reveal soil-stream DIC linkages in contrasting headwater catchments. J. Geophys. Res. Biogeosci. 123, 149–167. https://doi.org/10.1002/2017JG004083.

Celle-Jeanton, H., Emblanch, C., Mudry, J., Charmoille, A., 2003. Contribution of time tracers (Mg2+, TOC, D13CTDIC, NO3-) to understand the role of the unsaturated zone: a case study—Karst aquifers in the Doubs valley, eastern France. Geophys. Res. Lett. 30. https://doi.org/10.1029/2002GL016781.

Cerling, T.E., Solomon, D.K., Quade, J., Bowman, J.R., 1991. On the isotopic composition of carbon in soil carbon dioxide. Geochim. Cosmochim. Acta 55, 3403–3405. https://doi.org/10.1016/0016-7037(91)90498-T.

Chasar, L.S., Chanton, J.P., Glaser, P.H., Siegel, D.I., Rivers, J.S., 2000. Radiocarbon and stable carbon isotopic evidence for transport and transformation of dissolved organic carbon, dissolved inorganic carbon, and CH4 in a northern Minnesota peatland. Glob. Biogeochem. Cycles 14, 1095–1108. https://doi.org/10.1029/1999GB001221.

Collin, L., 2016. Établissement d'un Modèle Conceptuel du Fonctionnement Hydro-Écologique de la Tourbière de Frasne (Master Degree, Internship Report). Université de Franche-Comté - Communauté de Communes du Plateau de Frasne et du Val du Drugeon.

Colombié, C., Lécuyer, C., Strasser, A., 2011. Carbon- and oxygen-isotope records of palaeoenvironmental and carbonate production changes in shallow-marine carbonates (Kimmeridgian, Swiss Jura). Geol. Mag. 148, 133–153. https://doi.org/10.1017/S0016756810000518.

Conrad, R., 2020. Importance of hydrogenotrophic, aceticlastic and methylotrophic methanogenesis for methane production in terrestrial, aquatic and other anoxic environments: a mini review. Pedosphere 30, 25–39. https://doi.org/10.1016/S1002-0160(18)60052-9.

Corbett, J.E., Tfaily, M.M., Burdige, D.J., Cooper, W.T., Glaser, P.H., Chanton, J.P., 2013. Partitioning pathways of CO2 production in peatlands with stable carbon isotopes. Biogeochemistry 114, 327–340. https://doi.org/10.1007/s10533-012-9813-1.

D'Angelo, B., Leroy, F., Guimbaud, C., Jacotot, A., Zocatelli, R., Gogo, S., Laggoun-Défarge, F., 2021. Carbon balance and spatial variability of CO2 and CH4 fluxes in a sphagnum-dominated peatland in a temperate climate. Wetlands 41, 5. https://doi.org/10.1007/s13157-021-01411-y.

Deines, P., Langmuir, D., Harmon, R.S., 1974. Stable carbon isotope ratios and the existence of a gas phase in the evolution of carbonate ground waters. Geochim. Cosmochim. Acta 38, 1147–1164. https://doi.org/10.1016/0016-7037(74)90010-6.

Deirmendjian, L., Abril, G., 2018. Carbon dioxide degassing at the groundwater-stream-atmosphere interface: isotopic equilibration and hydrological mass balance in a sandy watershed. J. Hydrol. 558, 129–143. https://doi.org/10.1016/j.jhydrol.2018.01.003.

Delarue, F., Laggoun-Défarge, F., Buttler, A., Gogo, S., Jassey, V.E.J., Disnar, J.-R., 2011. Effects of short-term ecosystem experimental warming on water-extractable organic matter in an ombrotrophic Sphagnum peatland (Le Forbonnet, France). Org. Geochem. 42, 1016–1024. https://doi.org/10.1016/j.orggeochem.2011.07.005.

Dinsmore, K.J., Billett, M.F., Skiba, U.M., Rees, R.M., Drewer, J., Helfter, C., 2010. Role of the aquatic pathway in the carbon and greenhouse gas budgets of a peatland catchment: C and GHG release through peatland streams. Glob. Chang. Biol. 16, 2750–2762. https://doi.org/10.1111/j.1365-2486.2009.02119.x.

Dunfield, P., Knowles, R., Dumont, R., Moore, T., 1993. Methane production and consumption in temperate and subarctic peat soils: Response to temperature and pH. Soil Biol. Biochem. 25, 321–326. https://doi.org/10.1016/0038-0717(93)90130-4.

Duraffourg, M., Palacio, P., 1981. Etude Géologique, Géophysique, Géotechnique et Hydrologique du Synclinal de Frasne-Bonnevaux (Doubs) (Thèse). Université de Franche-Comté, Besançon.

Emblanch, C., Blavoux, B., Puig, J.-M., Couren, M., 1998. Le marquage de la zone non saturée du karst à l'aide du carbone 13. C. R. Acad. Sci. Ser. IIA Earth Planet. Sci. 326, 327–332. https://doi.org/10.1016/S1251-8050(98)80302-9.

Emblanch, C., Zuppi, G.M., Mudry, J., Blavoux, B., Batiot, C., 2003. Carbon 13 of TDIC to quantify the role of the unsaturated zone: the example of the Vaucluse karst systems (Southeastern France). J. Hydrol. 279, 262–274. https://doi.org/10.1016/S0022-1694(03)00180-X.

Fierz, S., Monbaron, M., 1999. Morphogenèse des Franches-Montagnes (Jura Suisse). Eclogae Geol. Helv. 199–210. https://doi.org/10.5169/SEALS-168661.

Gaillardet, J., Braud, I., Hankard, F., Anquetin, S., Bour, O., Dorfliger, N., de Dreuzy, J.R., Galle, S., Galy, C., Gogo, S., Gourcy, L., Habets, F., Laggoun, F., Longuevergne, L., Le Borgne, T., Naaim-Bouvet, F., Nord, G., Simonneaux, V., Six, D., Tallec, T., Valentin, C., Abril, G., Allemand, P., Arènes, A., Arfib, B., Arnaud, L., Arnaud, N., Arnaud, P., Audry, S., Comte, V.B., Batiot, C., Battais, A., Bellot, H., Bernard, E., Bertrand, C., Bessière, H., Binet, S., Bodin, J., Bodin, X., Boithias, L., Bouchez, J., Boudevillain, B., Moussa, I.B., Branger, F., Braun, J.J., Brunet, P., Caceres, B., Calmels, D., Cappelaere, B., Celle-Jeanton, H., Chabaux, F., Chalikakis, K., Champollion, C., Copard, Y., Cotel, C., Davy, P., Deline, P., Delrieu, G., Demarty, J., Dessert, C., Dumont, M., Emblanch, C., Ezzahar, J., Estèves, M., Favier, V., Faucheux, M., Filizola, N., Flammarion, P., Floury, P., Fovet, O., Fournier, M., Francez, A.J., Gandois, L., Gascuel, C., Gayer, E., Genthon, C., Gérard, M.F., Gilbert, D., Gouttevin, I., Grippa, M., Gruau, G., Jardani, A., Jeanneau, L., Join, J.L., Jourde, H., Karbou, F., Labat, D., Lagadeuc, Y., Lajeunesse, E., Lastennet, R., Lavado, W., Lawin, E., Lebel, T., Le Bouteiller, C., Legout, C., Lejeune, Y., Le Meur, E., Le Moigne, N., Lions, J., Lucas, A., Malet, J.P., Marais-Sicre, C., Maréchal, J.C., Marlin, C., Martin, P., Martins, J., Martinez, J.M., Massei, N., Mauclerc, A., Mazzilli, N., Molénat, J., Moreira-Turcq, P., Mougin, E., Morin, S., Ngoupayou, J.N., Panthou, G., Peugeot, C., Picard, G., Pierret, M.C., Porel, G., Probst, A., Probst, J.L., Rabatel, A., Raclot, D., Ravanel, L., Rejiba, F., René, P., Ribolzi, O., Riotte, J., Rivière, A., Robain, H., Ruiz, L., Sanchez-Perez, J.M., Santini, W., Sauvage, S., Schoeneich, P., Seidel, J.L., Sekhar, M., Sengtaheuanghoung, O., Silvera, N., Steinmann, M., Soruco, A., Tallec, G., Thibert, E., Lao, D.V., Vincent, C., Viville, D., Wagnon, P., Zitouna, R., 2018. OZCAR: the French network of critical zone observatories. Vadose Zone J. 17, 0. https://doi.org/10.2136/vzj2018.04.0067.

Galand, P.E., Fritze, H., Conrad, R., Yrjälä, K., 2005. Pathways for methanogenesis and diversity of methanogenic archaea in three boreal peatland ecosystems. Appl. Environ. Microbiol. 71, 2195–2198. https://doi.org/10.1128/AEM.71.4.2195-2198.2005.

Galand, P.E., Yrjälä, K., Conrad, R., 2010. Stable carbon isotope fractionation during methanogenesis in three boreal peatland ecosystems. Biogeosciences 7, 3893–3900. https://doi.org/10.5194/bg-7-3893-2010.

Garrels, R.M., Christ, C.L., 1965. Solutions, Minerals, and Equilibria. Harper & Row. Ed, New York.

Gauci, V., Dise, N., Fowler, D., 2002. Controls on suppression of methane flux from a peat bog subjected to simulated acid rain sulfate deposition: acid rain SO_4^{2-} suppression of CH_4 flux. Glob. Biogeochem. Cycles 16, 4–1–4–12. https://doi.org/10.1029/2000GB001370.

Gauthier, E., Jassey, V.E.J., Mitchell, E.A.D., Lamentowicz, M., Payne, R., Delarue, F., Laggoun-Defarge, F., Gilbert, D., Richard, H., 2019. From climatic to anthropogenic drivers: a multi-proxy reconstruction of vegetation and peatland development in the French Jura mountains. Quaternary 2, 38. https://doi.org/10.3390/quat2040038.

Gillon, M., Barbecot, F., Gibert, E., Corcho Alvarado, J.A., Marlin, C., Massault, M., 2009. Open to closed system transition traced through the TDIC isotopic signature at the aquifer recharge stage, implications for groundwater 14C dating. Geochim. Cosmochim. Acta 73, 6488–6501. https://doi.org/10.1016/j.gca.2009.07.032.

Goldscheider, N., Chen, Z., Auler, A.S., Bakalowicz, M., Broda, S., Drew, D., Hartmann, J., Jiang, G., Moosdorf, N., Stevanovic, Z., Veni, G., 2020. Global distribution of carbonate rocks and karst water resources. Hydrogeol. J. 28, 1661–1677. https://doi.org/10.1007/s10040-020-02139-5.

Gorham, E., 1991. Northern peatlands: role in the carbon cycle and probable responses to climatic warming. Ecol. Appl. 1, 182–195. https://doi.org/10.2307/1941811.

Goubet, P., 2015. Résultat d'expertise de l'analyse des Macrorestes de Carottes de Tourbe de la Tourbière Active de Frasne (25, France).

Graven, H., Keeling, R.F., Rogelj, J., 2020. Changes to carbon isotopes in atmospheric CO_2 over the industrial era and into the future. Glob. Biogeochem. Cycles 34. https://doi.org/10.1029/2019GB006170.

Hartmann, J., Moosdorf, N., 2012. The new global lithological map database GLiM: a representation of rock properties at the Earth surface: TECHNICAL BRIEF. Geochem. Geophys. Geosyst. 13. https://doi.org/10.1029/2012GC004370.

Holmes, M.E., Chanton, J.P., Tfaily, M.M., Ogram, A., 2015. CO2 and CH4 isotope compositions and production pathways in a tropical peatland. Glob. Biogeochem. Cycles 29, 1–18. https://doi.org/10.1002/2014GB004951.

Hornibrook, E.R.C., Longstaffe, F.J., Fyfe, W.S., 1997. Spatial distribution of microbial methane production pathways in temperate zone wetland soils: Stable carbon and hydrogen isotope evidence. Geochim. Cosmochim. Acta 61, 745–753. https://doi.org/10.1016/S0016-7037(96)00368-7.

Ingram, H.A.P., 1978. Soil layers in mires: function and terminology. J. Soil Sci. 29, 224–227. https://doi.org/10.1111/j.1365-2389.1978.tb02053.x.

Ingram, H.A.P., 1982. Size and shape in raised mire ecosystems: a geophysical model. Nature 297, 300–303. https://doi.org/10.1038/297300a0.

Jacotot, A., Bertrand, Guillaume, Toussaint, Marie-Laure, Lhosmot, Alexandre, Gilbert, Daniel, Binet, Philippe, Gogo, Sébastien, Laggoun-Défarge, Fatima, 2021. Carbon and Energy Eddy-Covariance Fluxes Dataset Collected at Frasne Peatland (192ha, Jura Mountains, France). https://doi.org/10.5281/ZENODO.4584507.

Jeannin, P.-Y., Hessenauer, M., Malard, A., Chapuis, V., 2016. Impact of global change on karst groundwater mineralization in the Jura Mountains. Sci. Total Environ. 541, 1208–1221. https://doi.org/10.1016/j.scitotenv.2015.10.008.

Joachimski, M.M., 1994. Subaerial exposure and deposition of shallowing upward sequences: evidence from stable isotopes of Purbeckian peritidal carbonates (basal cretaceous), Swiss and French Jura Mountains. Sedimentology 41, 805–824. https://doi.org/10.1111/j.1365-3091.1994.tb01425.x.

Koebsch, F., Winkel, M., Liebner, S., Liu, B., Westphal, J., Schmiedinger, I., Spitzy, A., Gehre, M., Jurasinski, G., Köhler, S., Unger, V., Koch, M., Sachs, T., Böttcher, M.E., 2019. Sulfate deprivation triggers high methane production in a disturbed and rewetted coastal peatland. Biogeosciences 16, 1937–1953. https://doi.org/10.5194/bg-16-1937-2019.

Komor, S.C., 1994. Geochemistry and hydrology of a calcareous fen within the Savage Fen wetlands complex, Minnesota, USA. Geochim. Cosmochim. Acta 58, 3353–3367. https://doi.org/10.1016/0016-7037(94)90091-4.

Lamers, L.P.M., Farhoush, C., Van Groenendael, J.M., Roelofs, J.G.M., 1999. Calcareous groundwater raises bogs; the concept of ombrotrophy revisited. J. Ecol. 87, 639–648. https://doi.org/10.1046/j.1365-2745.1999.00380.x.

Langmuir, D., 1971. The geochemistry of some carbonate ground waters in central Peale. Geochim. Cosmochim. Acta 35, 1023–1045. https://doi.org/10.1016/0016-7037(71)90019-6.

Langmuir, D., 1997. Aqueous Environmental Geochemistry. Prentice Hall, Upper Saddle River, N.J.

Lansdown, J.M., Quay, P.D., King, S.L., 1992. CH4 production via CO2 reduction in a temperate bog: a source of 13C-depleted CH4. Geochim. Cosmochim. Acta 56, 3493–3503.

Laudon, H., Berggren, M., Ågren, A., Buffam, I., Bishop, K., Grabs, T., Jansson, M., Köhler, S., 2011. Patterns and dynamics of dissolved organic carbon (DOC) in boreal streams: the role of processes, connectivity, and scaling. Ecosystems 14, 880–893. https://doi.org/10.1007/s10021-011-9452-8.

Lhosmot, A., Collin, L., Magnon, G., Steinmann, M., Bertrand, C., Stefani, V., Toussaint, M., Bertrand, G., 2021. Restoration and meteorological variability highlight nested water supplies in middle altitude/latitude peatlands: Towards a hydrological conceptual model of the Frasne peatland, Jura Mountains, France. Ecohydrology 14. https://doi.org/10.1002/eco.2315.

Lhosmot, Alexandre, Jacotot, Adrien, Steinmann, Marc, Binet, Philippe, Toussaint, Marie-Laure, Gogo, Sébastien, Gilbert, Daniel, Coffinet, Sarah, Laggoun-Deffarge, Fatima, Bertrand, Guillaume, 2022. Biotic and Abiotic Control Over Diurnal CH4 Fluxes in a Temperate Transitional Poor Fen Ecosystem. Ecosystems. https://doi.org/10.1007/s10021-022-00809-x.

Limpens, J., Berendse, F., Blodau, C., Canadell, J.G., Freeman, C., Holden, J., Roulet, N., Rydin, H., Schaepman-Strub, G., 2008. Peatlands and the Carbon Cycle: From Local Processes to Global Implications – A Synthesis. p. 17.

Loisel, J., Garneau, M., Hélie, J.-F., 2010. Sphagnum δ13C values as indicators of palaeohydrological changes in a peat bog. The Holocene 20, 285–291. https://doi.org/10.1177/0959683609350389.

Loisel, J., Gallego-Sala, A.V., Amesbury, M.J., Magnan, G., Anshari, G., Beilman, D.W., Benavides, J.C., Blewett, J., Camill, P., Charman, D.J., Chawchai, S., Hedgpeth, A., Kleinen, T., Korhola, A., Large, D., Mansilla, C.A., Müller, J., van Bellen, S., West, J.B., Yu, Z., Bubier, J.L., Garneau, M., Moore, T., Sannel, A.B.K., Page, S., Väliranta, M., Bechtold, M., Brovkin, V., Cole, L.E.S., Chanton, J.P., Christensen, T.R., Davies, M.A., De Vleeschouwer, F., Finkelstein, S.A., Frolking, S., Gałka, M., Gandois, L., Girkin, N., Harris, L.I., Heinemeyer, A., Hoyt, A.M., Jones, M.C., Joos, F., Juutinen, S., Kaiser, K., Lacourse, T., Lamentowicz, M., Larmola, T., Leifeld, J., Lohila, A., Milner, A.M., Minkkinen, K., Moss, P., Naafs, B.D.A., Nichols, J., O'Donnell, J., Payne, R., Philben, M., Piilo, S., Quillet, A., Ratnayake, A.S., Roland, T.P., Sjögersten, S., Sonnentag, O., Swindles, G.T., Swinnen, W., Talbot, J., Treat, C., Valach, A.C., Wu, J., 2021. Expert assessment of future vulnerability of the global peatland carbon sink. Nat. Clim. Chang. 11, 70–77. https://doi.org/10.1038/s41558-020-00944-0.

Luo, J., Li, S., Ni, M., Zhang, J., 2019. Large spatiotemporal shifts of CO2 partial pressure and CO2 degassing in a monsoonal headwater stream. J. Hydrol. 579, 124135. https://doi.org/10.1016/j.jhydrol.2019.124135.

Martin, J., De Grammont, P., Covington, M., Toran, L., 2021. A new focus on the neglected carbonate critical zone. Eos 102. https://doi.org/10.1029/2021EO163388.

McKenzie, J.M., Siegel, D.I., Rosenberry, D.O., Glaser, P.H., Voss, C.I., 2007. Heat transport in the Red Lake Bog, Glacial Lake Agassiz Peatlands. Hydrol. Process. 21, 369–378. https://doi.org/10.1002/hyp.6239.

Mook, W.G., Bommerson, J.C., Staverman, W.H., 1974. Carbon isotope fractionation between dissolved bicarbonate and gaseous carbon dioxide. Earth Planet. Sci. Lett. 22, 169–176. https://doi.org/10.1016/0012-821X(74)90078-8.

National Research Council, 2001. Basic Research Opportunities in Earth Science. National Academies Press, Washington, D.C. https://doi.org/10.17226/9981.

Neumann, R.B., Blazewicz, S.J., Conaway, C.H., Turetsky, M.R., Waldrop, M.P., 2016. Modeling CH4 and CO2 cycling using porewater stable isotopes in a thermokarst bog in Interior Alaska: results from three conceptual reaction networks. Biogeochemistry 127, 57–87. https://doi.org/10.1007/s10533-015-0168-2.

Nghiem, V.-T., 2006. Impact du Changement du Mode d'occupation des Sols Sur le Fonctionnement Hydrogéochimique des Grands Bassins Versants : cas du Bassin Versant de l'Ain. Université de Grenoble.

Preuss, I., Knoblauch, C., Gebert, J., 2012. Improved Quantification of Microbial CH4 Oxidation. Discussion Paper 37.

Reddy, K.R., DeLaune, R.D., 2008. Biogeochemistry of Wetlands: Science and Applications. CRC Press, Boca Raton.

Reeve, A.S., Siegel, D.I., Glaser, P.H., 1996. Geochemical controls on peatland pore water from the Hudson Bay Lowland: a multivariate statistical approach. J. Hydrol. 181, 285–304. https://doi.org/10.1016/0022-1694(95)02900-1.

Rosset, Thomas, Binet, S., Antoine, J.-M., Lerigoleur, E., Rigal, F., Gandois, L., 2019a. Drivers of seasonal and event scale DOC dynamics at the outlet of mountainous peatlands revealed by high frequency monitoring (preprint). Biogeochem.: Wetlands. https://doi.org/10.5194/bg-2019-372.

Rosset, T., Gandois, L., Le Roux, G., Teisserenc, R., Durantez Jimenez, P., Camboulive, T., Binet, S., 2019b. Peatland contribution to stream organic carbon exports from a montane watershed. J. Geophys. Res. Biogeosci. 124, 3448–3464. https://doi.org/10.1029/2019JG005142.

Sizova, M.V., Panikov, N.S., Tourova, T.P., Flanagan, P.W., 2003. Isolation and characterization of oligotrophic acido-tolerant methanogenic consortia from a Sphagnum peat bog. FEMS Microbiol. Ecol. 45, 301–315. https://doi.org/10.1016/S0168-6496(03)00165-X.

Steinmann, P., Shotyk, W., 1997. Geochemistry, mineralogy, and geochemical mass balance on major elements in two peat bog profiles (Jura Mountains, Switzerland). Chem. Geol. 138, 25–53. https://doi.org/10.1016/S0009-2541(96)00171-4.

Steinmann, P., Eilrich, B., Leuenberger, M., Burns, S.J., 2008. Stable carbon isotope composition and concentrations of CO2 and CH4 in the deep catotelm of a peat bog. Geochim. Cosmochim. Acta 72, 6015–6026. https://doi.org/10.1016/j.gca.2008.09.024.

Still, C.J., Berry, J.A., Collatz, G.J., DeFries, R.S., 2003. Global distribution of C3 and C4 vegetation: Carbon cycle implications. Glob. Biogeochem. Cycles 17, 6–1–6–14. https://doi.org/10.1029/2001GB001807.

Sullivan, P.L., Macpherson, G.L., Martin, J.B., Price, R.M., 2019. Evolution of carbonate and karst critical zones. Chem. Geol. 527, 119223. https://doi.org/10.1016/j.chemgeo.2019.06.023.

Throckmorton, H.M., Heikoop, J.M., Newman, B.D., Altmann, G.L., Conrad, M.S., Muss, J.D., Perkins, G.B., Smith, L.J., Torn, M.S., Wullschleger, S.D., Wilson, C.J., 2015. Pathways and transformations of dissolved methane and dissolved inorganic carbon in Arctic tundra watersheds: evidence from analysis of stable isotopes: dissolved CH_4 AND CO_2 in Arctic Tundra. Glob. Biogeochem. Cycles 29, 1893–1910. https://doi.org/10.1002/2014GB005044.

Toussaint, M.-L., Bertrand, G., Lhosmot, A., Gilbert, D., Binet, P., Jacotot, A., Gogo, S., Laggoun-Defarge, F., 2020. Soil-Meteorological Dataset Collected at Frasne Peatland (192ha, Jura Mountains, France). https://doi.org/10.5281/ZENODO.3763342.

Urban, N., Verry, E.S., Eisenreich, S., Grigam, D.F., Sebestyen, S.D., 2011. Element cycling in upland/peatland watersheds. In: Peatland Biogeochemistry and Watershed

Hydrology at the Marcell Experimental Forest. p. 29.
Vogel, J.C., Grootes, P.M., Mook, W.G., 1970. Isotopic fractionation between gaseous and dissolved carbon dioxide. Z. Physik 230, 225–238. https://doi.org/10.1007/BF01394688.
Wallin, M., Buffam, I., Öquist, M., Laudon, H., Bishop, K., 2010. Temporal and spatial variability of dissolved inorganic carbon in a boreal stream network: Concentrations and downstream fluxes: temporal and spatial variability of DIC. J. Geophys. Res. 115. https://doi.org/10.1029/2009JG001100. . n/a-n/a.
Whiticar, M.J., Faber, E., Schoell, M., 1986. Biogenic methane formation in marine and freshwater environments: CO2 reduction vs. acetate fermentation—Isotope evidence. Geochim. Cosmochim. Acta 50, 693–709. https://doi.org/10.1016/0016-7037(86)90346-7.
Wigley, T.M.L., Plummer, L.N., Pearson, F.J., 1978. Mass transfer and carbon isotope evolution in natural water systems. Geochim. Cosmochim. Acta 42, 1117–1139. https://doi.org/10.1016/0016-7037(78)90108-4.
Xu, X., Elias, D.A., Graham, D.E., Phelps, T.J., Carroll, S.L., Wullschleger, S.D., Thornton, P.E., 2015. A microbial functional group-based module for simulating methane production and consumption: Application to an incubated permafrost soil: a microbial functional group-based methane module. J. Geophys. Res. Biogeosci. 120, 1315–1333. https://doi.org/10.1002/2015JG002935.
Xu, J., Morris, P.J., Liu, J., Holden, J., 2018. PEATMAP: refining estimates of global peatland distribution based on a meta-analysis. CATENA 160, 134–140. https://doi.org/10.1016/j.catena.2017.09.010.
Ye, R., Jin, Q., Bohannan, B., Keller, J.K., McAllister, S.A., Bridgham, S.D., 2012. pH controls over anaerobic carbon mineralization, the efficiency of methane production, and methanogenic pathways in peatlands across an ombrotrophic–minerotrophic gradient. Soil Biol. Biochem. 54, 36–47. https://doi.org/10.1016/j.soilbio.2012.05.015.
Zhong, Y., Jiang, M., Middleton, B.A., 2020. Effects of water level alteration on carbon cycling in peatlands. Ecosys. Health Sustainabil. 6, 1806113. https://doi.org/10.1080/20964129.2020.1806113.